Levantine Journal of Applied Sciences, Volume 4 (1) (2024) 1-11

Levantine Journal of Applied Sciences

journal homepage: https://www.ljoas.com

Gamma radiation shielding features of Bismuth Germanate glasses doped Rare-earth ions using PHITS Monte Carlo code

Mustafa Hicabi Bölükdemir [1], Erhan Eser [2] and Hüseyin Koç [3*]

[1]*Department of Physics, Faculty of Sciences, Gazi University, Ankara, Türkiye*
[2]*Department of Physics, Polatlı Faculty of Arts and Sciences, Ankara Hacı Bayram Veli University, Ankara, Türkiye*
[3]*Department of Electrical and Electronics Engineering, Faculty of Engineering, Muş Alparslan University, Muş, Türkiye*

(Orcid: 0000-0002-7911-7863, Orcid: 0000-0003-3207-818X, Orcid: 0000-0002-3552-6227)

Keywords

Radiation shielding
Bismuth Germanate
Mass attenuation coefficient
Buildup factors
Monte Carlo

ABSTRACT

In this work, mass attenuation coefficient, effective atomic number, effective electron density, the mean free path, and buildup factor of Bismuth germanate glasses with different densities have been calculated using the PHITS MC code and the XCOM program in the energy region from 1.5 keV to 15 MeV. In the calculations, a mathematical expression determining the sample thickness depending on the incident photon energy (for E≤ 1.25 MeV) was derived by considering the optimization criterion. For E> 1.25 MeV, it was observed that the thickness value could be between 4 and 10 cm and did not affect the determination of the MAC. The MAC from MC and XCOM were in good agreement with each other. It was found to be around 0.044 cm2/g above 1 MeV, while HVL was found to be 2.2 cm. At the absorption edge of Bismuth, the results obtained also show that the buildup factor increases with the increasing density of the bismuth germanate.

1. Introduction

The study of the radiation interaction with matter is important in many scientific and industrial applications, especially in the field of radiological engineering for reactor design where radiation exposure is controlled using suitable shielding materials for indirect ionizing particles like gamma-ray. These particles become the primary problem for radiation shielding in nuclear facilities because they do not interact well with matter (Kaplan, 1989). It is therefore important to develop a mixture of materials that can be used as a shield against nuclear radiation (Saeed et al., 2014; V. P. Singh et al., 2014; Sayyed and Elhouichet., 2017; Gökmen, 2022; Almuqrin and Sayyed, 2021). Given this, glasses as shielding materials are promising materials because of their homogeneity, simplicity to manufacture, melting point properties, and high transparency (Chanthima et al., 2012; Sayyed and Elhouichet, 2017; K.J. Singh et al., 2008). Adding oxide to the glass formulation can increase the radiation protection properties of glasses (Chanthima et al., 2012; Eskalen et al., 2020; Kavun et al., 2022).

The different types of glass systems such as bismuth borate glasses, lead borate glasses, barium-borate-flyash glasses, glasses containing Bi_2O_3, PbO, and BaO, barium-bismuth-borosilicate glasses, bismuth borosilicate glasses, heavy-metal oxide glasses ($Bi_4Ge_3O_{12}$, Gd_2SiO_5Ce, and $ZnWO_4$), and boro-tellurite glasses as shielding materials and their radiation shielding properties have been studied and reported by many researchers in the literature (AbuAlRoos et al., 2019; El-Rehim et al., 2021; Elbashir et al., 2018; Kurudirek et al., 2018; Mahapatra and Barai, 2018; V.P. Singh et al., 2014; K. Singh et al., 2005; N. Singh et al., 2006; S. Singh et al., 2008; Tekin et al., 2017) . Among several glass systems, oxide glasses have recently gained a lot attention because of their most stable active ion host for practical applications, mainly due to their high chemical durability and thermal stability (Sayyed et al., 2019a; Sayyed and Elhouichet, 2017; V.P. Singh et al., 2014). Among them, heavy metal oxide glasses are especially well-suitable materials to reduce the intensity and energy of the gamma radiation due to their high refractive index, high

* Corresponding author.
Email address: huseyinnkoc@yahoo.com (H.Koç)
http://dx.doi.org/10.56917/ljoas.20

density, high optical susceptibility, high infrared transparency, high interaction cross-section, and good radiation shielding properties (V.P. Singh et al., 2014). Adding heavy metal oxides to glass systems makes them more chemically stable and devitrification resistant (Çelikbilek et al., 2013; Fares et al., 2014).

With its excellent scintillation, piezoelectric and optical properties, $Bi_4Ge_3O_{12}$ (Bismuth Germanate, BGO), one of the most important heavy metal oxide glasses, is a well-known scintillation material and shows the luminescence in the near-ultraviolet and visible spectral ranges excited by ionizing electromagnetic radiation or charged particles (electrons, protons, ions) (Koshimizu et al., 2017; Kuz'Micheva et al., 2020a). It is therefore widely used in practical applications such as medicine (Albarzan et al., 2021; Hampel, 2015; Kozma and Kozma, 2003; Valais et al., 2010), high energy physics (Grigoriev et al., 2014), and geological surveys (Dias et al., 2016). BGO can block x- and gamma photons while transmitting photons in the visible region, making it preferred in critical studies or space studies where electromagnetic waves are observed. The development of BGO with various rare-earth ions (Eu^{+3}, Er^{+3}, Nd^{+3}, Dy^{+3}, etc.) (Huang et al., 2021; Karabulut et al., 2016; Kuz'Micheva et al., 2020a; Polosan, 2019) and nanoparticle synthesis (Oviedo et al., 2016) continues.

In this study, we calculated the mass attenuation coefficients, half-value layer, mean free path, the effective atomic number, the effective electron density, and buildup factor for gamma-ray shielding properties of BGO glasses with different densities in the energy range of 1.5 keV–15 MeV using the PHITS MC code and the XCOM program. Additionally, Z_{eff} and <Z> values were calculated by using the molar fraction, atomic mass, and mass attenuation coefficients of each element forming the compounds. The present investigation results are useful for gamma-ray, and design for suitable lead-free shielding material in radiological engineering.

2. Material and Method

2.1. Bismuth Germanate

Many studies in the literature involve Bismuth Germanate ($Bi_4Ge_3O_{12}$ or BGO) with different properties, but in this study, only three samples with relatively different densities were selected, whose the density and atomic weight content of compound are known as necessary for the Monte Carlo calculation. The BGO-1 sample is BGO with a density of 7.13 g/cm^3, which has a high stopping power for high energy photons and is used in radiation detection as reported in the literature (Grigoryeva and Salakhutdinov, 2020; Koshimizu et al., 2017). BGO-2 is a colored (pink) BGO sample obtained using milligrams of stannous oxalate SnC_2O_4 by Kuz'micheva et al.(2018) and its density is 7.168 g/cm^3. The BGO-3 sample is the sample coded BGO:0.1% Dy synthesized by Kuz'micheva et al. (2020b). Its density is 7.377 g/cm^3. They grew an optically homogeneous $Bi_4Ge_3O_{12}$ single crystal doped with Dy_2O_3 (Kuz'Micheva et al., 2020a). All $Bi_4Ge_3O_{12}$ crystals had been grown by the Czochralski method. Atomic weight fractions of selected $Bi_4Ge_3O_{12}$ crystals are given in Table 1.

Table 1 Densities and weight fraction of each element in the $Bi_4Ge_3O_{12}$ samples.

Sample code	Density g/cm^3	Bi	Ge	O	Dy
BGO-	7.13	0.67102	0.17485	0.154119	None
BGO-	7.16	0.67102	0.17485	0.154119	None
BGO-	7.37	0.67035	0.17468	0.154094	0.00087

2.2. Mass Attenuation Coefficient

Almost all material types can be used for gamma-ray shielding at a given thickness. However, the radiation attenuation properties of materials are highly dependent on the density of the shielding material, atomic number, and electron density. As a parallel beam of monochromatic gamma-ray photons (narrow beam geometry) propagates through the shielding material, the beam intensity, *I*, decreases according to the Lambert-Beer law.

$$I = I_0 e^{-\frac{\mu}{\rho}\rho t} \quad (1)$$

where I_0 is the incident intensity of radiation, *I* is the attenuated photon intensity, *t* (cm) is the sample thickness, μ (cm^{-1}) is the linear attenuation coefficient of the shielding material, and ρ (g/cm^3) is the measured density of a sample. μ depends on the elemental or chemical composition and the density of the sample. Generally, the mass attenuation coefficient (MAC), μ/ρ, which is independent of density and can be obtained by dividing μ by density, is preferred, and its unit is cm^2/g. μ/ρ is one of the important parameters for evaluating the shielding properties of materials (Hubbell and Seltzer, 2004; Seltzer, 1993). The higher it is in a particular material, the better it attenuates photons.

The MAC of a mixture shielding material at a certain photon energy is the sum of the products of the weight fraction and the MAC of the element *i* at that energy (Kavun et al., 2022), namely,

$$\left(\frac{\mu}{\rho}\right)_t = \sum_i w_i \left(\frac{\mu}{\rho}\right)_i \quad (2)$$

where $w_i = \frac{n_i A_i}{\sum_i n_i A_i}$ is the weight fraction of the ith element, n_i is the number of atoms of the ith constituent element and is assumed to be an integer, and A_i is the atomic mass. The total weight fraction should be $\sum_i w_i = 1$.

The MAC can be obtained from XCOM computer programs (Berger et al., 2010), from Windows successor WinXCom (Gerward et al., 2004), or various Monte Carlo codes. Using these programs, the MAC can be calculated as needed for any element, compound, or mixture at any energy between 1 keV and 100 GeV.

2.3. Effective atomic number and Electron density

To know the interaction of the photon in the matter, the total photon interaction cross-section per molecule must first be known. The total photon interaction cross-section per at each

element is proportional to the MAC (μ/ρ).

$$Z_{eff} = \frac{\sum_i f_i A_i \left(\frac{\mu}{\rho}\right)_i}{\sum_j f_j \frac{A_j}{Z_j}\left(\frac{\mu}{\rho}\right)_j} \quad (3)$$

where $f_i (= \frac{n_i}{n})$ is a molar fraction and is expressed in units of atomic percentage and $\sum_j f_j = 1$. It is the general description for calculating the Z_{eff} for all types of materials, compounds, and mixtures (Manohara et al., 2008a). It is the general description for calculating the Z_{eff} for all types of materials, compounds, and mixtures (Manohara et al., 2008a). It can be seen that $(1/Z_{eff})$ is the weighted arithmetic mean of $(1/Z_i)$, where the weighting factor associated with each element is $n_i A_i (\mu/\rho)_i$. Eq. (3) gives a more general relation in molar fraction (f_i) and can be used for calculating Z_{eff} of both compounds and mixtures. Z_{eff} is an energy-dependent quantity.

The Z_{eff} is closely related to the electron density Ne, expressed as the number of electrons per unit mass. The electron density for a chemical element is given by $N_e = N_A Z/A$. If N_e is to be written for a compound,

$$N_e = N_A \frac{Z_{eff}}{\langle A \rangle} . \quad (4)$$

where $\langle A \rangle = \frac{\sum_i n_i A_i}{n}$ is the mean atomic mass of the compound. The mean atomic number of the compounds is $\langle Z \rangle = \frac{\sum_i n_i Z_i}{n}$. Where the actual photon interaction process is Compton scattering, $Z_{eff} = \langle Z \rangle$. $\langle Z \rangle$ can be used instead of Z_{eff} in Eq. (4).

2.4. Mean Free Path and Half Value Layer

The linear attenuation coefficients are obtained by multiplying the MAC with respect to the energy by the density of the target. The mean free path (MFP) also called the relaxation length is the average distance a photon can travel in the material before interacting.

$$\text{MFP} = {}^{1}/_{\mu} . \quad (5)$$

Half-value layer (HVL) is the material thickness that halves the intensity of the incident photon.

$$\text{HVL} = {}^{\ln 2}/_{\mu} . \quad (6)$$

Both quantities are in cm. In this study, XCOM and PHITS MC codes were used to obtain the MAC of each sample at 47 different photon energies in the range of 1.5 keV to 15 MeV. The energy-related MFP and HVL values are obtained by multiplying them by the material density.

2.5. Buildup Factors

For most practical applications, good geometry is not the case, as is the Lambert-Beer law. Therefore, this law is modified to account for multiple scattering of photons (ie. broad geometry),

$$I = BI_0 e^{-\frac{\mu}{\rho}\rho t} . \quad (7)$$

where the correction factor *B* is unitless and is called the buildup factor. *B* describes the ratio of the broad beam to the narrow beam. In geometries where the Lambert-Beer assumption is valid, *B* is equal to 1, otherwise, *B* is always greater than 1. *B* is a function of the photon energy and the depth of penetration, usually expressed as the MFP. It is an important parameter for assessing the thickness of the material in radiation shielding because it directly affects the absorbed radiation dose.

Evaluation of photon buildup factors by GP fitting depends on obtaining 5 fitting parameters (b, c, a, X_k, and d) that depend on Z_{eq} and photon energy (P. S. Singh et al., 2008).

The scattering and absorption of photons from any material are characterized by the photoelectric effect, Compton scattering, and pair-production coefficients. These interactions depend on the photon energies and the atomic number of the medium. The atomic number describes both the material properties of an element and its radiation interaction-related properties. Z_{eq} is synonymous with the atomic number of an element for a multi-element material and represents the weighted average of electrons per atom. Z_{eq}, Compton partial interaction coefficient $(\mu/\rho)_{Comp}$ and total MAC $(\mu/\rho)_t$ (both in cm^2/g) are obtained and then the $R = (\mu/\rho)_{Comp}/(\mu/\rho)_t$ ratio of the material in question is obtained. It is calculated at the photon energy of interest. Interpolate using the Z_{eq} expression (Harima, 1983):

$$Z_{eq} = \frac{Z_1(logR_2 - logR) + Z_2(logR - logR_1)}{(logR_2 - logR_1)} \quad (8)$$

where Z_1 and Z_2 are the atomic numbers of elements corresponding to the $(\mu/\rho)_{Comp}/(\mu/\rho)_t$ ratios, R_1 and R_2, respectively. R is the ratio for the selected sample at a particular energy such that $R_1 < R < R_2$ (Singh et al., 2008).

In this study, ExabCal, which is a Windows compatible program (Olarinoye et al., 2019), was used to calculate the energy absorption buildup factor (EABF) of the samples. It considers photon energies in the range of 15 keV- 15 MeV. It calculates buildup factors based on the well-known Geometric Progression (GP) fitting procedure (Harima, 1983; P.S. Singh et al., 2008). Z_{eq} and GP fitting parameters of mixtures and compounds can also be evaluated using this program.

2.6. Monte Carlo Simulation by PHITS Code

Monte Carlo (MC) particle transport simulation codes are an important tool used in many research areas where radiation interaction, especially radiation shielding and protection. General-purpose MC codes adopted in the literature are MCNP (Issa et al., 2018; Kumar et al., 2018; Sayyed et al., 2018), Geant4 (Boonin et al., 2020; Boukhris et al., 2020; Sayyed et al., 2019a), Fluka (Boukhris et al., 2020; Boonin et al., 2020; Al-Buriahi et al., 2020), Penelope (Sandev, 2010), and also

PHITS (Particle and Heavy Ion Transport Code System) is a successful particle transport simulation code that is increasingly used (Al-Buriahi et al., 2020; Sriwunkum and Nutaro, 2019). PHITS is a code that can handle most types of particles with energies up to 1 TeV (per nucleon per ion) using several nuclear reaction models and data libraries (Sato et al., 2018). It was used to obtain the photon fluence rate in a certain region in PHITS. The T-track tally evaluates the trace length whenever particles pass through a certain region, and the sum of the track lengths is scored in cm. Narrow beam transmission geometric simulation was performed to investigate the photon attenuation coefficients of BGO samples using PHITS version 3.2.

The schematic diagram of the PHITS simulation geometry is shown in Fig. 1 in 2D. The photon beam source was defined to be 66 cm from the face of the detector as a 0.25 cm radius disc source inside the cylindrical Pb shield, and the photons were allowed to propagate along the cylindrical axis. The detector considered in this simulation is a NaI crystal with a crystal height of 7.62 cm and a diameter of 7.62 cm, which is also widely used in the literature (Akkurt et al., 2020; Shi et al., 2002; Sriwunkum and Nutaro, 2019). BGO samples of various thicknesses (t) were placed between the radiation source, detector, and lead collimators with a 0.4 cm aperture placed to collimate the beam in narrow geometry.

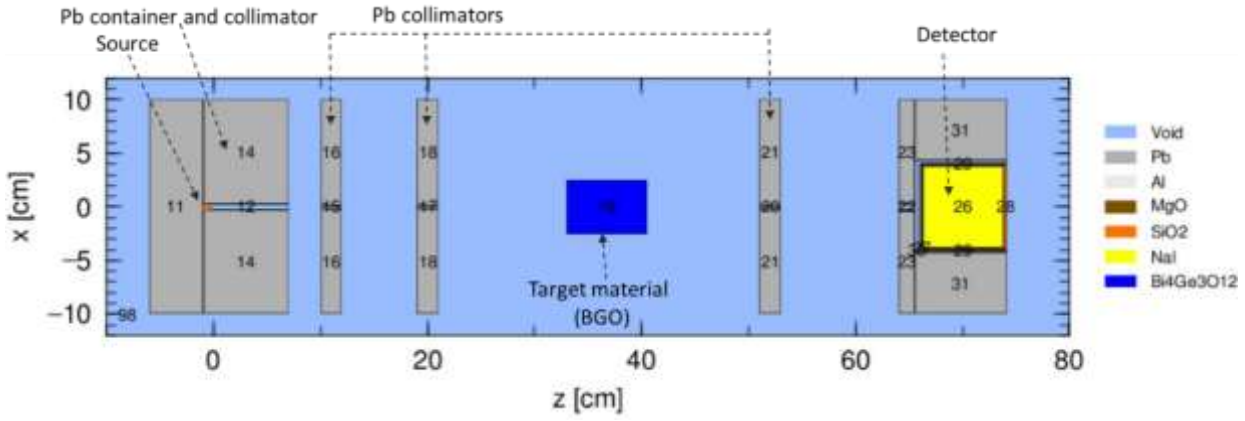

Fig. 1. A 2D view of PHITS simulation geometry.

The thickness (*t*) of the sample has been optimized according to the gamma-ray energy chosen, i.e. unkept constant. The optimization criterion (Creagh and Hubbell, 1987) was applied to determine the thickness of the target material as follows.

$$2 \leq ln\left(\frac{I_0}{I}\right) \leq 4 \qquad (9)$$

Thus, it is ensured that not all photons are absorbed by the material or pass through the material without any interaction. In this study, the history number for each simulation is 10^6 and the tally results have a statistical error of less than 0.77%.

3. Results and Discussion

Table 1 shows the sample code, density, and weight fraction of each element of the BGO heavy oxide crystals considered in this study. MAC of each BGO was calculated using the XCOM program in the energy range of 1.5 keV to 15 MeV. Also, the gamma shielding studies of BGOs were achieved by determining the MAC values by using the PHITS MC code. Considering the Creagh and Hubbell optimization criterion and the MAC in the range of 1.5keV-15MeV from XCOM for BGO samples, it was decided that it would be appropriate to express the optimum thickness values depending on the energy. A graph of possible sample thickness *t* (*E*) with respect to energy was plotted and fitted to determine a function. As a result, the thickness was determined as a function of energy as follows and used in PHITS calculations. For values greater than $E \geq 1.25$ MeV for the lower and upper limits of the Creagh and Hubbell criterion, it was observed that the *t* value could be between 4 and 10 cm and did not affect the determination of the MAC. Therefore, the sample thickness was taken as a constant for the energy region of 1.25 MeV < E < 15 MeV.

$$t(E) = \begin{cases} exp\left(-4.02 + 6.33\ cos(0.31\ log(E) - 0.54)\right) & for\ \ E \leq 1.25MeV \\ 7.5cm & for\ E > 1.25MeV \end{cases} \qquad (10)$$

The results of PHITS and XCOM and the relative percent deviation (*RD*%) between them are shown in Table 2. *RD*% was estimated using the following equation.

$$RD\% = \frac{|MAC_{XCOM} - MAC_{PHITS}|}{MAC_{XCOM}} \times 100 \qquad (11)$$

Table 2 MACs (cm^2/g) of the BGO samples obtained by XCOM and PHITS simulations with different photons energies, and relative % deviations from each other.

Energy MeV	BGO-1			BGO-2			BGO-3		
	XCOM	PHITS	RD%	XCOM	PHITS	RD%	XCOM	PHITS	RD%
0.0015	2852	2856.66	0.16	2852	2857.25	0.18	2854	2860.80	0.24
0.002	1485	1484.15	0.06	1485	1484.00	0.07	1487	1485.92	0.07
0.00277	1515	1475.88	2.58	1515	1475.60	2.60	1515	1475.40	2.61
0.003	1579	1569.99	0.57	1579	1570.10	0.56	1579	1569.71	0.59
0.00322	1547	1544.23	0.18	1547	1544.14	0.18	1546	1544.60	0.09
0.00377	1064	1124.84	5.72	1064	1124.73	5.71	1064	1124.25	5.66
0.004	962.8	965.29	0.26	962.8	965.08	0.24	962.5	964.32	0.19
0.005	559.2	561.48	0.41	559.2	561.63	0.44	559	561.47	0.44
0.006	356.5	356.99	0.14	356.5	357.00	0.14	356.4	356.65	0.07
0.008	173.4	173.22	0.10	173.4	173.26	0.08	173.6	173.35	0.14
0.01	98.72	98.46	0.26	98.72	98.44	0.28	98.87	98.54	0.33
0.0111	105.4	106.28	0.84	105.4	106.28	0.83	105.5	106.30	0.75
0.01342	65.3	64.51	1.21	65.3	64.50	1.23	65.36	64.56	1.23
0.01571	83.3	83.25	0.06	83.3	83.23	0.08	83.3	83.21	0.11
0.01644	112	113.39	1.25	112	113.41	1.26	112	113.30	1.16
0.02	67.58	67.53	0.07	67.58	67.53	0.08	67.55	67.51	0.06
0.03	23.63	23.69	0.27	23.63	23.69	0.27	23.62	23.67	0.21
0.04	11.16	11.16	0.02	11.16	11.16	0.01	11.15	11.16	0.10
0.05	6.238	6.222	0.25	6.238	6.222	0.25	6.235	6.224	0.18
0.06	3.894	3.872	0.57	3.894	3.872	0.57	3.902	3.881	0.54
0.08	1.884	1.856	1.51	1.884	1.855	1.52	1.888	1.858	1.59
0.09053	1.393	1.346	3.36	1.393	1.346	3.36	1.395	1.349	3.27
0.1	3.971	3.967	0.10	3.971	3.966	0.14	3.970	3.969	0.03
0.15	1.462	1.461	0.09	1.462	1.461	0.10	1.461	1.459	0.12
0.2	0.742	0.741	0.05	0.742	0.741	0.06	0.741	0.741	0.10
0.3	0.316	0.315	0.21	0.316	0.315	0.23	0.316	0.315	0.30
0.4	0.192	0.191	0.43	0.192	0.191	0.39	0.192	0.191	0.42
0.5	0.139	0.138	0.56	0.139	0.138	0.55	0.139	0.138	0.54
0.6	0.111	0.111	0.46	0.111	0.111	0.46	0.111	0.111	0.46
0.8	0.083	0.083	0.16	0.083	0.083	0.13	0.083	0.083	0.16
1.022	0.067	0.067	0.31	0.067	0.067	0.30	0.067	0.067	0.25
1.25	0.058	0.056	3.37	0.058	0.056	3.40	0.058	0.056	3.53
1.5	0.052	0.052	0.53	0.052	0.052	0.52	0.052	0.052	0.47
2.044	0.045	0.045	1.31	0.045	0.046	1.32	0.045	0.045	1.21
3	0.040	0.041	1.92	0.040	0.041	1.92	0.040	0.041	1.86
4	0.039	0.040	2.27	0.039	0.040	2.24	0.039	0.040	2.12
6	0.039	0.040	2.26	0.039	0.040	2.27	0.039	0.040	2.15
8	0.041	0.041	2.08	0.041	0.041	2.06	0.041	0.041	2.05
10	0.042	0.043	1.89	0.042	0.043	1.88	0.042	0.043	1.79
12	0.044	0.045	1.63	0.044	0.045	1.62	0.044	0.045	1.57
14	0.046	0.047	1.46	0.046	0.047	1.44	0.046	0.047	1.37
15	0.0478	0.0489	1.29	0.0478	0.0489	1.30	0.0478	0.0489	1.29

Except for the edge energies of the elements in BGOs, the average RD% for below 1.25 MeV energies is below 0.8%, while above 1.25 MeV it is 1.58% (see Table 2). The edge energies of the bismuth are 90.53 keV for the K-edge; 16.39 keV, 15.71 keV, 13.42 keV for L-edge; 3.70 keV, 3.18 keV, 2.69 keV for the M-edge. Those of germanium are 11.10 keV for the K-edge; 1.41 keV, and 1.22 keV for the L-edge. The obtained results reveal that the difference between theoretical values (XCOM) and simulated values (PHITS) excluding edge energies is less than 3%, confirming the accuracy of the present results. Determining the target thickness as a function of photon energy causes the difference in edge energies to reach 6%, but this difference is not an unacceptable value since it is observed at a few energies. The energy-dependent variation of MAC for the three BGO samples with different density is shown in Fig. 2. As seen in Fig.2, PHITS results are in good agreement with XCOM. As Table 2 and Fig. 2 are shown, there is a maximum deviation of 0.2% between the MAC of the BGOs. That is, the density difference is not large enough to produce a difference between the MAC values. In addition to, the MAC values are very high for each BGO in the low energies. For instance, at 0.015 MeV, it is about 2850 cm^2/g.

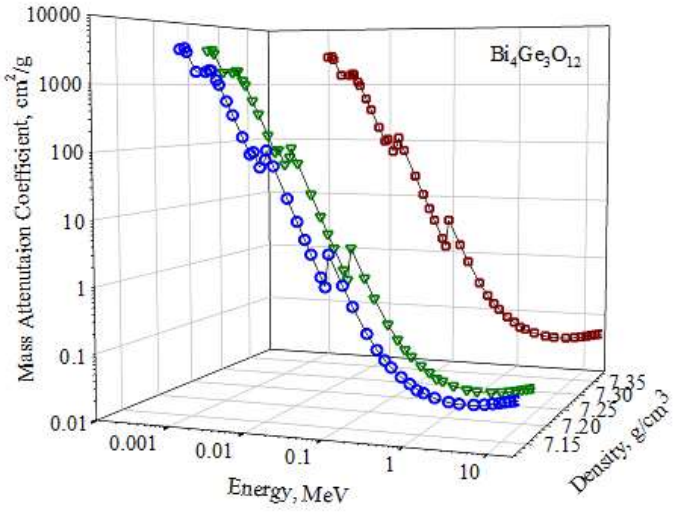

Fig. 2. Profiles of MAC according to incident photon energy for selected BGO samples. Solid lines are data from XCOM, signs are from PHITS.

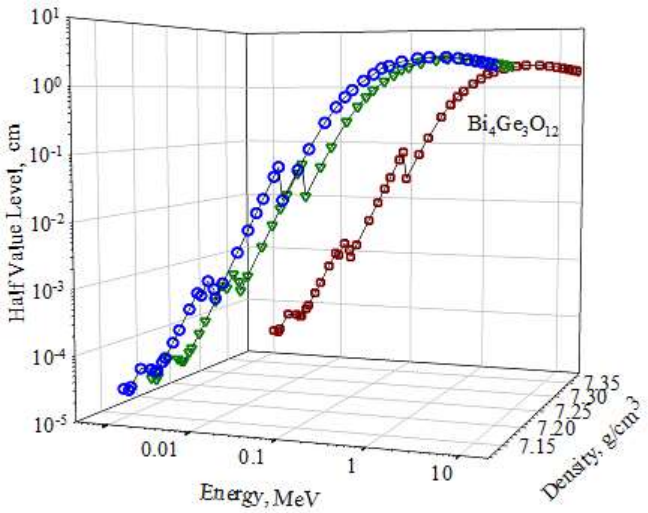

Fig. 3. Profiles of HVL according to incident photon energy for selected BGO samples. Solid lines are derived from XCOM, signs are from PHITS.

The MAC value decreases swiftly up to 0.5 MeV energy, then it slows down, and after 1 MeV there is an increase again. This can be explained by photon partial interaction processes. In the low energy region (0.5MeV and below), the attenuation is inversely proportional to E^3 with photon energy due to the predominance of photoelectric absorption, and proportional to Z^4 with the atomic number of a target, while in the high energy region (1.022 MeV and above) it increases in proportion to E with the pair production process (Martin, 2006). In the intermediate region, Compton scattering dominates the attenuation process and is inversely proportional to E. For these reasons, since BGOs contain high Z elements such as Bi, their MAC values reach their maximum values at low energies. MAC values of BGO are higher than concretes and window glasses in Sayyed et al., (2019b), that is, BGO glasses have suitable efficiency in terms of gamma photon shielding, and considering these results, BGO glasses with suitable composition can be developed for use as a radiation shielding material.

Fig. 3 shows the energy dependence of HVL, while Fig. 4 shows the effect on HVL of increasing density relative to the smallest density, and the HVL value decreases with increasing density. The HVL values of BGOs start from 0.34 μm at 0.015 MeV and reach their maximum value at 2.42 cm at 4 MeV and decline to 1.99 cm at 15 MeV. HVL is expected to be low for shielding. BGOs in this form show better results than HVL values of Bi-containing composites (Sayyed et al., 2019b). Compared to BGO-1, the HVL of BGO-2 decreased by 0.5% on average, while that of BGO-3 decreased by an average of 3.3%. The MFP is a measure of the average distance traveled by the photon between two successive interactions. Fig. 5 represents the results of the MFP variation as a function of energy. MFP profile seen in Fig. 5 shows a similar behavior with HVL as expected.

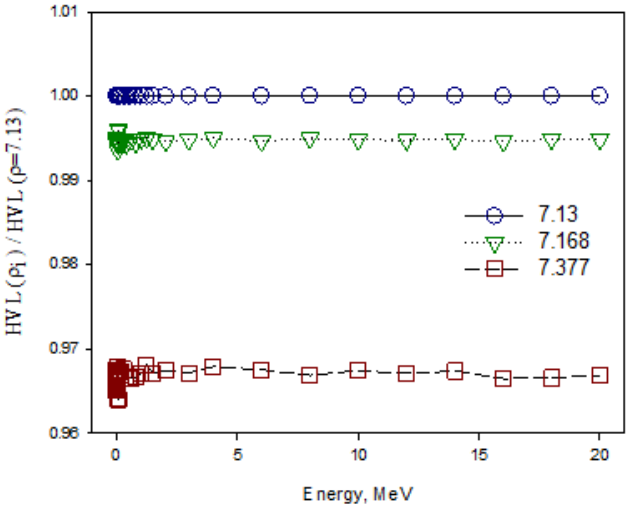

Fig. 4. HVL ratios of BGOs by energy.

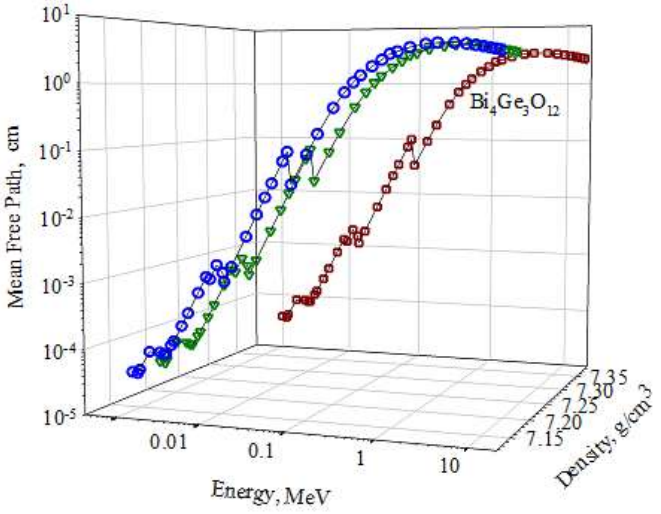

Fig. 5. Profile of the mean free path according to a photon energy of BGO samples with different densities.

Z_{eff} obtained from the calculated MAC values is important for predicting how photons interact with a substance, as certain photon interactions depend on the atomic number. To test the usability of BGOs in gamma shielding applications, Z_{eff} was calculated and given as a function of photon energy in Fig. 6. Z_{eff} for the BGOs presented here are not density-dependent. The Z_{eff} values of $Bi_4Ge_3O_{12}$: 0.1% Dy_2O_3 and the BGO-1 crystal differ from each other by an average of 0.02% differences, so only BGO-1 was plotted. Fig.6 shows four energy regions: below 0.005 MeV, 0.005–0.1 MeV, 0.1-1MeV and above 1 MeV. In the first energy zone, it rapidly increases from 32 to 66. While Z_{eff} ranges from 66-70 in the second region, an initial discontinuous rise in the third region, followed by a quick fall with increasing energy, and a rapid increase in the fourth region is observed. Considering the photon partial interaction processes, the first region suggests photoelectric absorption, the second region presents a mixed transition of photoelectric and incoherent (Compton) scattering; the third region presents the transition to incoherent (Compton) scattering; it is clear that more than 1.022 MeV pair-production is dominant and the process causes Z_{eff} increase with energy. The 0.1-1 MeV range is the transition region without pure Compton scattering, where Z_{eff} decreases rapidly with energy increase, in this region, the main interaction process shifts from photoelectric absorption to pair-production as energy increases. Z_{eff} has a discontinuous jump at 2.69 keV, 13.42 keV, and 90.53 keV. This is because the Bi element inside the target has an M, L, and K absorption edge, respectively. The presence of absorption edges makes the applicability of the Z_{eff} somewhat problematic at certain energies. This view is in agreement with that of Manohara et al.(2008a). Having high Z_{eff} values of a sample means that the photon absorption ability is also high and therefore there will be better photon shielding performance for the sample. The high-Z Bi element increases the Z_{eff} of BGOs, thus increasing the photon shielding performance.

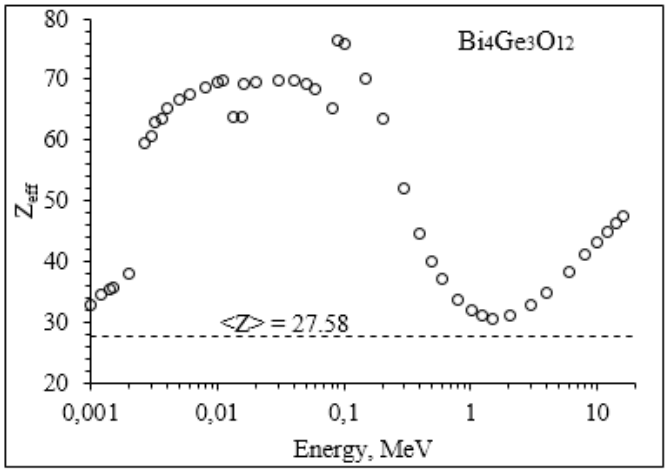

Fig. 6. Effective atomic number versus photon energy.

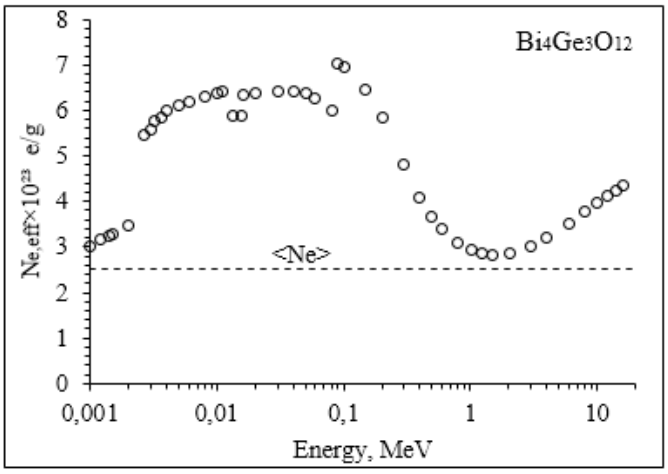

Fig. 7. Electron density versus photon energy.

The variation of the Z_{eq} of BGOs depending on the photon energy is shown in Fig. 8. The Z_{eq} values of BGO-3 and the BGO-1 crystal differ from each other by an average of 1.0% difference, so only BGO-1 was plotted. Z_{eq} is independent of mass density, as Z_{eff}. Considering the Fig. 8 as three energy regions: Z_{eq} slowly increases from 70 to 76 depending on lnE as the energy increases in the mid-energy range of 0.1-2.0 MeV (Compton scattering). Unlike Z_{eff}, Z_{eq} slowly decreases with an increase in energy in the region above 1 MeV (pair production). Unlike Z_{eff}, in the region above 1 MeV, Z_{eq} slowly decreases with an increase in energy. Z_{eq} is affected by the photoelectric effect and pair production processes, while Z_{eff} is affected by Compton scattering and pair production.

The EABF of BGOs for incident photon energies in the 0.015–15 MeV range up to 1, 3, 5, and 10 MFP penetration depths were calculated. The energy dependence of EABF for BGO-1 is given in Fig.9. The EABF values of BGO-1 and -2 were obtained the same. Since the only difference between the two samples is the mass density, the EABF is not density-dependent in the energy range of interest. As the MFP value increases above 0.1 MeV photon energy, the EABF decomposes and increases with energy in the 0.2-1.0 MeV energy range, that is, in the Compton scattering region, except for 1MFP. A decrease is observed in EABF up to 8 MeV above 1MeV, while a significant increase is observed over 8 MeV photon energy as MFP increases. This means that as the thickness of the samples of interest increases, the number of photons absorbed increases, on the other hand, leakage radiation is important at small MFP values.

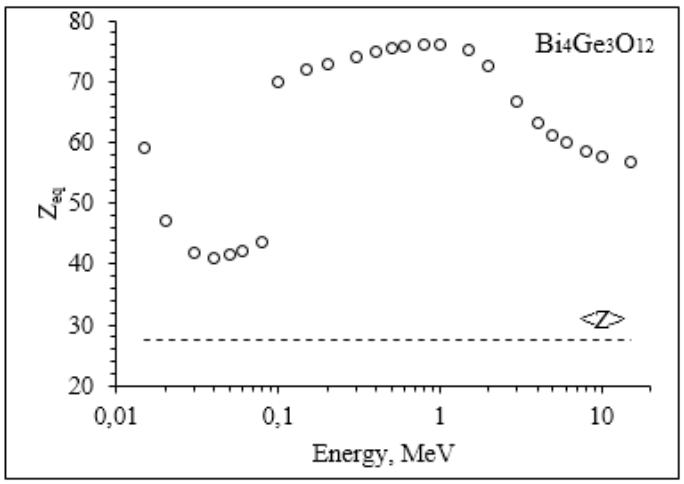

Fig. 8. Equivalent atomic number versus photon energy.

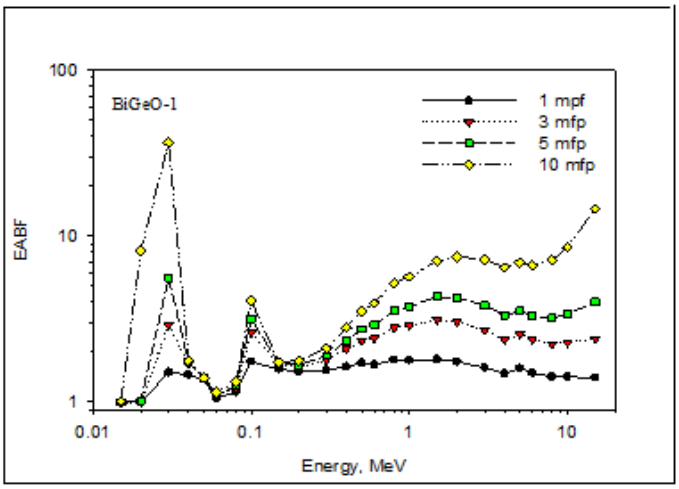

Fig. 9. Energy absorption build-up factor versus energy.

The EABF comparison of BGO-1 and -3 is given in Fig. 10 as the ratio of each other. At 0.2 MeV and above this ratio is about 1.0, so the EABF for each BGO is the same. Below 0.2 MeV there is a divergence at 0.1 MeV, 0.06 MeV and 0.03 MeV. This energy region is dominated by the photoelectric effect, so the absorption edges can be seen as responsible. The difference between BGO-1 and -3 is that BGO-3 has a Dy atom and Dy has a K-edge energy of 53.79 keV. This result may explain the difference at relatively 0.06 MeV, but the increase in divergence at 0.1 MeV and 0.03 MeV with MFP suggests that there is a mixed photon interaction process in this region.

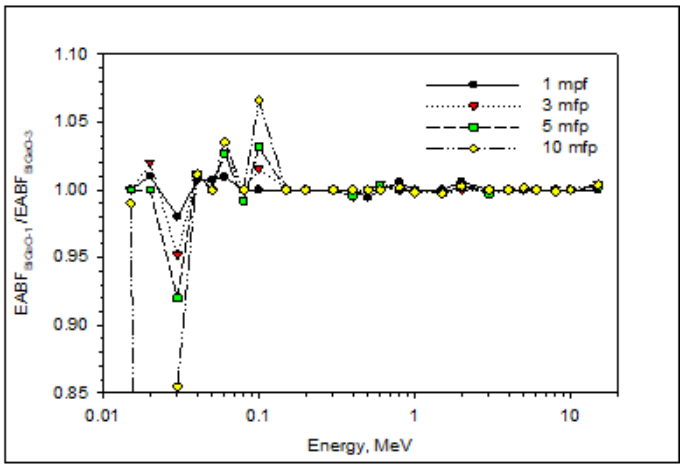

Fig. 10. Ratio of energy absorption build-up factor from BGO-1 to that from BGO-3.

4. Conclusions

In this study, it has been reported that three Bismuth Germanate crystalline glasses with different densities can serve in radiation protection applications. The MAC required for the radiation shielding properties was determined for each sample in the photon energy range of 1.5 keV–15 MeV using the PHITS MC code and the XCOM program. In the calculations carried out with the MC code, a mathematical expression determining the sample thickness depending on the incident photon energy was derived by considering the optimization criterion. A sample thickness of about three MFP is optimal for determining the MAC for photon energies below 1.25 MeV. For more than 1.25 MeV, this value is taken into account as 2.5 MFP. We observed that the MC results obtained using this method were in good agreement with XCOM. Z_{eff} is greater than the mean atomic number in all energy ranges. This result indicates that there is no pure Compton scattering. A very sharp peak was observed in the EABF at 30 keV and 0.1MeV for BGO-1 and 2, while a peak at 60 keV was also observed for BGO-3.

Declaration of Competing Interest

The authors declare that they have no known competing financial interests or personal relationships that could have appeared to influence the work reported in this paper.

Cite this article: *Bölükdemir, M.H., Eser, E., Koç, H., 2024. Gamma radiation shielding features of Bismuth Germanate glasses doped Rare-earth ions using PHITS Monte Carlo code. Levantine Journal of Applied Sciences, Volume 4 (1), 1-10.* http://dx.doi.org/10.56917/ljoas.20

References

AbuAlRoos, N.J., Baharul Amin, N.A., Zainon, R., 2019. Conventional and new lead-free radiation shielding materials for radiation protection in nuclear medicine: A review. Radiation Physics and Chemistry 165, 108439. https://doi.org/10.1016/j.radphyschem.2019.108439

Akkurt, İ., Waheed, F., Akyildirim, H., Gunoglu, K., 2020. Monte Carlo simulation of a NaI(Tl) detector efficiency. Radiation Physics and Chemistry 176, 109081. https://doi.org/10.1016/j.radphyschem.2020.109081

Al-Buriahi, M.S., Sriwunkum, C., Arslan, H., Tonguc, B.T., Bourham, M.A., 2020. Investigation of barium borate glasses for radiation shielding applications. Applied Physics A: Materials Science and Processing 126, 1–9. https://doi.org/10.1007/s00339-019-3254-9

Albarzan, B., Almuqrin, A.H., Koubisy, M.S., Wahab, E.A.A., Mahmoud, K.A., Shaaban, K.S., Sayyed, M.I., 2021. Effect of Fe2O3 doping on structural, FTIR and radiation shielding characteristics of aluminium-lead-borate glasses. Progress in Nuclear Energy 141, 103931. https://doi.org/10.1016/j.pnucene.2021.103931

Almuqrin, A.H., Sayyed, M.I., 2021. Radiation shielding characterizations and investigation of TeO2–WO3–Bi2O3 and TeO2–WO3–PbO glasses. Applied Physics A: Materials Science and Processing 127, 1–11. https://doi.org/10.1007/s00339-021-04344-9

Berger, M.J., Hubbell, J.H., Seltzer, S.M., Chang, J., Coursey, J.S., Sukumar, R., Zucker, D.S., Olsen, K., 2010. XCOM: Photon Cross Section Database (version 1.5). [Online] Available: http://physics.nist.gov/xcom [2021, November 20] [WWW Document]. National Institute of Standards and Technology, Gağthersburg, MD. https://doi.org/https://dx.doi.org/10.18434/T48G6X

Boonin, K., Yasaka, P., Limkitjaroenporn, P., Rajaramakrishna, R., Askin, A., Sayyed, M.I., Kothan, S., Kaewkhao, J., 2020. Effect of BaO on lead free zinc barium tellurite glass for radiation shielding materials in nuclear application. Journal of Non-Crystalline Solids 550, 120386. https://doi.org/10.1016/j.jnoncrysol.2020.120386

Boukhris, I., Al-Buriahi, M.S., Akyildirim, H., Alalawi, A., Kebaili, I., Sayyed, M.I., 2020. Chalcogenide glass-ceramics for radiation shielding applications. Ceramics International 46, 19385–19392. https://doi.org/10.1016/j.ceramint.2020.04.281

Çelikbilek, M., Ersundu, A.E., Aydin, S., 2013. Preparation and characterization of TeO2-WO3-Li 2O glasses. Journal of Non-Crystalline Solids 378, 247–253. https://doi.org/10.1016/j.jnoncrysol.2013.07.020

Chanthima, N., Kaewkhao, J., Limsuwan, P., 2012. Study of photon interactions and shielding properties of silicate glasses containing Bi 2O 3, BaO and PbO in the energy region of 1 keV to 100 GeV. Annals of Nuclear Energy 41, 119–124. https://doi.org/10.1016/j.anucene.2011.10.021

Creagh, D.C., Hubbell, J.H., 1987. Problems Associated with the Measurement of X-ray Attenuation Coefficients. I. Silicon Report on the International Union of Crystallography X-ray Attenuation Project. Acta Crystallographica a43, 102–112. https://doi.org/https://doi.org/10.1107/S0108767387099793

Dias, F., Lima, M., Sanjurjo-Sánchez, J., Alves, C., 2016. Analysis of spectra from portable handheld gamma-ray spectrometry for terrain comparative assessment. Journal of Environmental Radioactivity 154, 93–100. https://doi.org/10.1016/j.jenvrad.2016.01.017

El-Rehim, A.F.A., Ali, A.M., Zahran, H.Y., Yahia, I.S., Shaaban, K.S., 2021. Spectroscopic, Structural, Thermal, and Mechanical Properties of B2O3-CeO2-PbO2 Glasses. Journal of Inorganic and Organometallic Polymers and Materials 31, 1774–1786. https://doi.org/10.1007/s10904-020-01799-w

Elbashir, B.O., Dong, M.G., Sayyed, M.I., Issa, S.A.M., Matori, K.A., Zaid, M.H.M., 2018. Comparison of Monte Carlo simulation of gamma ray attenuation coefficients of amino acids with XCOM program and experimental data. Results in Physics 9, 6–11. https://doi.org/10.1016/j.rinp.2018.01.075

Eskalen, H., Kavun, Y., Kerli, S., Eken, S., 2020. An investigation of radiation shielding properties of boron doped ZnO thin films. Optical Materials 105, 109871. https://doi.org/10.1016/j.optmat.2020.109871

Fares, H., Jlassi, I., Elhouichet, H., Férid, M., 2014. Investigations of thermal, structural and optical properties of tellurite glass with WO3 adding. Journal of Non-Crystalline Solids 396–397, 1–7. https://doi.org/10.1016/j.jnoncrysol.2014.04.012

Gerward, L., Guilbert, N., Jensen, K.B., Levring, H., 2004. WinXCom - A program for calculating X-ray attenuation coefficients. Radiation Physics and Chemistry 71, 653–654. https://doi.org/10.1016/j.radphyschem.2004.04.040

Gökmen, U., 2022. Gamma and neutron shielding properties of B4C particle reinforced Inconel 718 composites. Nuclear Engineering and Technology 54, 1049–1061. https://doi.org/10.1016/j.net.2021.09.028

Grigoriev, D.N., Danevich, F.A., Shlegel, V.N., Vasiliev, Y. V., 2014. Development of crystal scintillators for calorimetry in high energy and astroparticle physics. Journal of Instrumentation 9, C09004. https://doi.org/10.1088/1748-0221/9/09/C09004

Grigoryeva, I., Salakhutdinov, G., 2020. The use of scintillation crystals in nuclear medicine. Procedia Computer Science 169, 347–352. https://doi.org/10.1016/j.procs.2020.02.200

Hampel, U., 2015. In Industrial Tomography: Systems and Applications, M. Wang. ed. Woodhead Publishing, Cambridge.

Harima, Y., 1983. Approximation of Gamma-Ray Buildup Factors By Modified Geometrical Progression. Nuclear Science and Engineering 83, 299–309. https://doi.org/10.13182/NSE83-A18222

Huang, B., Zhang, B., Qian, X., Wang, J., Yang, Q., Su, L., 2021. Effects of Er3+ concentration on upconversion luminescence and temperature sensing properties in Bi4Ge3O12 crystal. Journal of Alloys and Compounds 853, 156970. https://doi.org/10.1016/j.jallcom.2020.156970

Hubbell, J.H., Seltzer, S.M., 2004. Tables of X-Ray Mass Attenuation Coefficients and Mass Energy-Absorption Coefficients from 1 keV to 20 MeV for Elements Z = 1 to 92 and 48 Additional Substances of Dosimetric Interest. NIST Standard Reference Database 126 21–22 https://doi.org/https://doi.org/10.1016/j.ecolecon.2013.02.003

Issa, S.A.M., Saddeek, Y.B., Tekin, H.O., Sayyed, M.I., Shaaban, K. saber, 2018. Investigations of radiation shielding using Monte Carlo method and elastic properties of PbO-SiO2-B2O3-Na2O glasses. Current Applied Physics 18, 717–727. https://doi.org/10.1016/j.cap.2018.02.018

Kaplan, M.F., 1989. Concrete Radiation Shielding, 1st ed. John Wiley & Sons, Inc., New York.

Karabulut, Y., Canimoglu, A., Ekdal, E., Ayvacikli, M., Can, N., Karali, T., 2016. Thermoluminescence studies of Nd doped Bi4Ge3O12 crystals irradiated by UV and beta sources. Applied Radiation and Isotopes 113, 18–21. https://doi.org/10.1016/j.apradiso.2016.04.004

Kavun, Y., Kerli, S., Eskalen, H., Kavgacı, M., 2022. Characterization and nuclear shielding performance of Sm doped In_2O_3 thin films. Radiation Physics and Chemistry 194, 110014. https://doi.org/10.1016/j.radphyschem.2022.110014

Koshimizu, M., Kurashima, S., Kimura, A., Taguchi, M., Yanagida, T., Fujimoto, Y., Asai, K., 2017. Analysis of linear energy transfer effects on the scintillation properties of Bi4Ge3O12 crystals. Nuclear Instruments and Methods in Physics Research, Section B: Beam Interactions with Materials and Atoms 409, 19–22. https://doi.org/10.1016/j.nimb.2017.04.010

Kozma, Peter, Kozma, Petr, 2003. Radiation resistivity of BGO

crystals due to low-energy gamma-rays. Nuclear Instruments and Methods in Physics Research, Section A: Accelerators, Spectrometers, Detectors and Associated Equipment 501, 499–504. https://doi.org/10.1016/S0168-9002(03)00617-X

Kumar, A., Sayyed, M.I., Dong, M., Xue, X., 2018. Effect of PbO on the shielding behavior of ZnO–P2O5 glass system using Monte Carlo simulation. Journal of Non-Crystalline Solids 481, 604–607. https://doi.org/10.1016/j.jnoncrysol.2017.12.001

Kurudirek, M., Chutithanapanon, N., Laopaiboon, R., Yenchai, C., Bootjomchai, C., 2018. Effect of Bi2O3 on gamma ray shielding and structural properties of borosilicate glasses recycled from high pressure sodium lamp glass. Journal of Alloys and Compounds 745, 355–364. https://doi.org/10.1016/j.jallcom.2018.02.158

Kuz'Micheva, G.M., Ivleva, L.I., Kaurova, I.A., Khramov, E. V., Dunaeva, E.E., Svetogorov, R.D., Rybakov, V.B., 2020a. Local structural features and composition of the Bi4Ge3O12:Dy3+crystals: Effect of doping concentration. CrystEngComm 22, 5666–5677. https://doi.org/10.1039/d0ce00729c

Kuz'Micheva, G.M., Ivleva, L.I., Kaurova, I.A., Khramov, E. V., Dunaeva, E.E., Svetogorov, R.D., Rybakov, V.B., 2020b. Local structural features and composition of the Bi4Ge3O12:Dy3+crystals: Effect of doping concentration. CrystEngComm 22, 5666–5677. https://doi.org/10.1039/d0ce00729c

Kuz'micheva, G.M., Kaurova, I.A., Ivleva, L.I., Khramov, E. V., Eistrikh-Geller, P.A., Rybakov, V.B., Chukhlovina, T. V., Firstov, S. V., 2018. Structure and composition peculiarities and spectral-luminescent properties of colorless and pink Bi4Ge3O12 scintillation crystals. Arabian Journal of Chemistry 11, 1270–1280. https://doi.org/10.1016/j.arabjc.2017.07.015

Mahapatra, C.K., Barai, S. V., 2018. Hybrid fiber reinforced self compacting concrete with fly ash and colloidal nano silica: A systematic study. Construction and Building Materials 160, 828–838. https://doi.org/10.1016/j.conbuildmat.2017.11.131

Manohara, S.R., Hanagodimath, S.M., Thind, K.S., Gerward, L., 2008a. On the effective atomic number and electron density: A comprehensive set of formulas for all types of materials and energies above 1 keV. Nuclear Instruments and Methods in Physics Research, Section B: Beam Interactions with Materials and Atoms 266, 3906–3912. https://doi.org/10.1016/j.nimb.2008.06.034

Manohara, S.R., Hanagodimath, S.M., Thind, K.S., Gerward, L., 2008b. On the effective atomic number and electron density: A comprehensive set of formulas for all types of materials and energies above 1 keV. Nuclear Instruments and Methods in Physics Research, Section B: Beam Interactions with Materials and Atoms 266, 3906–3912. https://doi.org/10.1016/j.nimb.2008.06.034

Martin, J.E., 2006. Interactions of Radiation with Matter, in: Physics of Radiation Protection. WILEY-VCH, Weinheim, pp. 305–363.

Olarinoye, I.O., Odiaga, R.I., Paul, S., 2019. EXABCal: A program for calculating photon exposure and energy absorption buildup factors. Heliyon 5, e02017. https://doi.org/10.1016/j.heliyon.2019.e02017

Oviedo, M.J., Contreras, O.E., Rosenstein, Y., Vazquez-Duhalt, R., Macedo, Z.S., Carbajal-Arizaga, G.G., Hirata, G.A., 2016. New Bismuth Germanate oxide nanoparticle material for biolabel applications in medicine. Journal of Nanomaterials 9782625. https://doi.org/10.1155/2016/9782625

Polosan, S., 2019. Crystallization processes in europium-doped Bi4Ge3O12 glass materials. Journal of Luminescence 213, 235–240. https://doi.org/10.1016/j.jlumin.2019.05.031

Saeed, A., El shazly, R.M., Elbashar, Y.H., Abou El-azm, A.M., El-Okr, M.M., Comsan, M.N.H., Osman, A.M., Abdal-monem, A.M., El-Sersy, A.R., 2014. Gamma ray attenuation in a developed borate glassy system. Radiation Physics and Chemistry 102, 167–170. https://doi.org/10.1016/j.radphyschem.2014.04.032

Sandev, T., 2010. Monte Carlo Simulation of Buildup Factors for Single and Multi-layer Shields by Using PENELOPE Code, in: Proc. of the Second Conference on Medical Physics and Biomedical Engineering. Skopje, Macedonia, pp. 72–77.

Sato, T., Iwamoto, Y., Hashimoto, S., Ogawa, T., Furuta, T., Abe, S., Kai, T., Tsai, P.E., Matsuda, N., Iwase, H., Shigyo, N., Sihver, L., Niita, K., 2018. Features of Particle and Heavy Ion Transport code System (PHITS) version 3.02. Journal of Nuclear Science and Technology 55, 684–690. https://doi.org/10.1080/00223131.2017.1419890

Sayyed, M.I., Aşkın, A., Ali, A.M., Kumar, A., Rashad, M., Alshehri, A.M., Singh, M., 2019a. Extensive study of newly developed highly dense transparent PbO-WO3-BaO-Na2O-B2O3 glasses for radiation shielding applications. Journal of Non-Crystalline Solids 521. https://doi.org/10.1016/j.jnoncrysol.2019.119521

Sayyed, M.I., Elhouichet, H., 2017. Variation of energy absorption and exposure buildup factors with incident photon energy and penetration depth for boro-tellurite (B2O3-TeO2) glasses. Radiation Physics and Chemistry 130, 335–342. https://doi.org/10.1016/j.radphyschem.2016.09.019

Sayyed, M.I., Kaky, K.M., Şakar, E., Akbaba, U., Taki, M.M., Agar, O., 2019b. Gamma radiation shielding investigations for selected germanate glasses. Journal of Non-Crystalline Solids 512, 33–40. https://doi.org/10.1016/j.jnoncrysol.2019.02.014

Sayyed, M.I., Rammah, Y.S., Abouhaswa, A.S., Tekin, H.O., Elbashir, B.O., 2018. ZnO-B2O3-PbO glasses: Synthesis and radiation shielding characterization. Physica B: Condensed Matter 548, 20–26. https://doi.org/10.1016/j.physb.2018.08.0241

Seltzer, S.M., 1993. Calculation of photon mass energy-transfer and mass energy-absorption coefficients. Radiation Research 136, 147–170. https://doi.org/10.2307/3578607

Sharma, A., Sayyed, M.I., Agar, O., Tekin, H.O., 2019. Simulation of shielding parameters for TeO 2 -WO 3 -GeO 2 glasses using FLUKA code. Results in Physics 13, 102199. https://doi.org/10.1016/j.rinp.2019.102199

Shi, H.X., Chen, B.X., Li, T.Z., Yun, D., 2002. Precise Monte Carlo simulation of gamma-ray response functions for an NaI(Tl) detector. Applied Radiation and Isotopes 57, 517–524. https://doi.org/10.1016/S0969-8043(02)00140-9

Singh, K., Singh, H., Sharma, G., Gerward, L., Khanna, A., Kumar, R., Nathuram, R., Sahota, H.S., 2005. Gamma-ray shielding properties of CaO-SrO-B 2O 3 glasses. Radiation Physics and Chemistry 72, 225–228. https://doi.org/10.1016/j.radphyschem.2003.11.010

Singh, K.J., Singh, N., Kaundal, R.S., Singh, K., 2008. Gamma-ray shielding and structural properties of PbO-SiO2 glasses. Nuclear Instruments and Methods in Physics Research, Section B: Beam Interactions with Materials and Atoms 266, 944–948. https://doi.org/10.1016/j.nimb.2008.02.004

Singh, N., Singh, K.J., Singh, K., Singh, H., 2006. Gamma-ray attenuation studies of PbO-BaO-B2O3 glass system. Radiation Measurements 41, 84–88. https://doi.org/10.1016/j.radmeas.2004.09.009

Singh, P.S., Singh, T., Kaur, P., 2008. Variation of energy absorption buildup factors with incident photon energy and penetration depth for some commonly used solvents. Annals of Nuclear Energy 35, 1093–1097. https://doi.org/10.1016/j.anucene.2007.10.007

Singh, S., Kumar, A., Singh, D., Thind, K.S., Mudahar, G.S., 2008. Barium-borate-flyash glasses: As radiation shielding materials. Nuclear Instruments and Methods in Physics Research, Section B: Beam Interactions with Materials and Atoms 266, 140–146. https://doi.org/10.1016/j.nimb.2007.10.018

Singh, V.P., Badiger, N.M., Kaewkhao, J., 2014. Radiation shielding competence of silicate and borate heavy metal oxide glasses:

Comparative study. Journal of Non-Crystalline Solids 404, 167–173. https://doi.org/10.1016/j.jnoncrysol.2014.08.003

Sriwunkum, C., Nutaro, T., 2019. Study on gamma-ray shielding properties of lead tellurite glass systems using PHITS. Journal of Physics: Conference Series 1380, 012138. https://doi.org/10.1088/1742-6596/1380/1/012138

Tekin, H.O., Singh, V.P., Manici, T., 2017. Effects of micro-sized and nano-sized WO3 on mass attenauation coefficients of concrete by using MCNPX code. Applied Radiation and Isotopes 121, 122–125. https://doi.org/10.1016/j.apradiso.2016.12.040

Valais, I.G., Michail, C.M., David, S.L., Liaparinos, P.F., Fountos, G.P., Paschalis, T. V., Kandarakis, I.S., Panayiotakis, G.S., 2010. Comparative investigation of Ce3+ doped scintillators in a wide range of photon energies covering X-ray CT, nuclear medicine and megavoltage radiation therapy portal imaging applications. IEEE Transactions on Nuclear Science 57, 3–7. https://doi.org/10.1109/TNS.2009.2038273